Introduction

Often, most time in the simulation of multi-phase flow through porous media is taken up by solution of the pressure equation. This involves primarily solving large systems of linear equations as part of the iterative solution of the time and space discretized governing nonlinear partial differential equations. The time spent in solving the linear systems depends on the size of the problem and the variations of permeability within the medium. Solution of problems with extreme contrast in the grid block permeability values may lead to very large computing times.
A potential approach to reduce the computing time for large-scale problems with the aid of Proper Orthogonal Decomposition (POD) is investigated in [1] and [5]. Astrid et al. [1] propose the use of a POD-based preconditioner for the acceleration of the solution to the pressure equation. The preconditioner is constructed from a set of snapshots, obtained from solutions to the pressure equation in previous time steps. Once the snapshots are computed, the POD method is used to obtain a set of basis vectors that capture the most relevant features of the system, which can be used to improve the simulation time of the subsequent time steps. A similar approach is used in [5], where a set of POD-based basis vectors is obtained from the initial time steps. However, in this case, the acceleration is achieved by only improving the initial guess.
Problems with a high contrast between the permeability coefficients are sometimes approached through the use of deflation techniques; see, e.g., [11]. The use of deflation techniques involves the search of good deflation vectors, which are usually problem-dependent. In [11], subdomain based deflation vectors are used for layered problems with a large contrast between the permeability coefficients. However, these deflation vectors cannot be used if the distribution of the permeability coefficients is not structured as is the case in, e.g., the well-known SPE 10 benchmark problem [3].
Following the ideas of [1] and [5], we propose the use of POD of many snapshots to capture the system's behavior. The basis obtained with POD is studied as an alternative choice of deflation vectors to accelerate the convergence of the pressure solution in a porous medium with high-contrast variations in the permeability coefficients. As a first step, we consider incompressible single-phase flow through porous media with large variations in the permeability coefficients for layered academic problems and the SPE 10 benchmark.

Method and/or Theory

Flow through porous media

We consider the semi-discretized form of the governing partial differential equations for single-phase flow, resulting in the system of ordinary differential equations [4],

$$\mathbf{V}\dot{\mathbf{p}} + \mathbf{T}\mathbf{p} = \mathbf{q}, \tag{1}$$

where $\mathbf{p}$ is a vector of grid block potentials, $\mathbf{q}$ is a vector of grid block source terms (wells), the dot represents differentiation with respect to time, $\mathbf{T}$ and $\mathbf{V}$ are the transmissibility and accumulation matrices. If we neglect gravity, the potential reduces to pressure, and if we furthermore restrict the analysis to slightly compressible flow, the system of differential equations (1) is linear. In case of large compressibilities or multiphase-flow, the equations are nonlinear but can be solved iteratively using the Newton-Raphson (NR) method.
To solve Equation (1) it is necessary to define initial conditions and boundary conditions. The latter conditions can be prescribed pressures (Dirichlet conditions), flow rates (Neumann conditions), or a combination of these (Robin conditions).
To represent the pressure drop resulting from sub-grid near-well flow convergence, and to allow for the prescription of pressures (rather than flow rates) in the wells we use the well-known Peaceman well model which changes Equation (1) into

$$\mathbf{V}\dot{\mathbf{p}} + \mathbf{T}\mathbf{p} = \mathbf{J}(\mathbf{p} - \mathbf{p}_{well}), \tag{2}$$

where $\mathbf{J}$ is a matrix with well indices in the appropriate positions and $\mathbf{p}_{well}$ is a vector of well bore pressures [4]. In case of incompressible flow, Equation (2) reduces to the system of algebraic equations

$$\mathbf{Tp} = \mathbf{J}(\mathbf{p} - \mathbf{p}_{well}). \tag{3}$$

Iterative solution methods

Equation (2) can be numerically integrated, for which the implicit Euler formulation is the most popular time discretization method in the reservoir simulation community. This results in a time stepping sequence that requires the solution of a system of linear equations at each time step:

$$\mathbf{Ax} = \mathbf{b}, \tag{4}$$

where the vector $\mathbf{x} = \mathbf{p}_{k+1}$, and where $\mathbf{A}$ and $\mathbf{b}$ can be expressed in terms of $\mathbf{p}_k$, $\mathbf{T}$, $\mathbf{V}$, $\mathbf{J}$ and $\mathbf{p}_{well}$ [4]. In case of a mass-conservative time discretization scheme for single-phase flow, $\mathbf{V}$ will be a function of $\mathbf{p}_{k+1}$, while in case of multi-phase flow also $\mathbf{T}$ and $\mathbf{J}$ become a function of $\mathbf{p}_{k+1}$. In those cases, system (4) will be the result of a NR procedure, and multiple instances of it need to be solved during a single time step until the NR procedure has converged. In case of incompressible flow, the linear system (4) results directly from rewriting Equation (3).
System (4) can be solved with direct or iterative methods. Direct methods achieve a final solution, while the iterative ones are stopped if the error is less than a given value.
For realistically sized reservoir problems the use of iterative solvers is usually the most efficient and often the only possible choice. Some well-known iterative methods are: Jacobi, Gauss Seidel and, if the matrix is Symmetric Positive Definite (SPD), the Conjugate Gradient (CG) method. Iterative methods can be preconditioned or deflated to accelerate the convergence. In the next section, we present the CG method, and we describe preconditioning and deflation techniques for the acceleration of this method.

Krylov subspace Methods

If we have two subspaces $\mathcal{K}_k$, $\mathcal{L}_k$ of $\mathbb{R}^n$ and we want to solve Equation (4), with $\mathbf{A} \in \mathbb{R}^{n\times n}$ we can use a projection method onto $\mathcal{K}_k$. This method allows us to find an approximate solution $\mathbf{x}^k$ from an arbitrary initial guess $\mathbf{x}^0$. This approximate solution lies in the Krylov subspace of dimension k of the matrix $\mathbf{A}$ and residual $\mathbf{r}^0$,

$$\mathbf{x}^k \in \mathbf{x}^0 + \mathcal{K}_k(\mathbf{A}, \mathbf{r}^0),$$

with $\mathcal{K}_k(\mathbf{A}, \mathbf{r}^0)$ defined as:

$$\mathcal{K}_k(\mathbf{A}, \mathbf{r}^0) = span\{\mathbf{r}^0, \mathbf{Ar}^0, \ldots, \mathbf{A}^{k-1}\mathbf{r}^0\},$$

where the residual $\mathbf{r}^k = \mathbf{b} - \mathbf{Ax}^k$ is orthogonal to the subspace $\mathcal{L}_k$, with

$$\mathbf{x}^{k+1} = \mathbf{x}^k + \mathbf{B}^{-1}r^k, \qquad \mathbf{r}^k = \mathbf{b} - \mathbf{Ax}^k.$$

The subspace $\mathcal{L}_k$ is chosen depending on the Krylov subspace method that is used.

Conjugate Gradient Method

The Conjugate Gradient (CG) method is a Krylov subspace method for *SPD* matrices, such that

$$||\mathbf{x} - \mathbf{x}^k||_{\mathbf{A}}{}^{1} \tag{5}$$

is minimal, with $\mathbf{x}$ the solution of the system and $\mathbf{x}^k$ the approximate solution after k iterations.
After $k+1$ iterations of the *CG* method, the error of the iteration is bounded by:

$$||\mathbf{x} - \mathbf{x}^{k+1}||_{\mathbf{A}} \leq 2||\mathbf{x} - \mathbf{x}^0||_{\mathbf{A}} \left(\frac{\sqrt{\mathbf{C}_2(\mathbf{A})} - 1}{\sqrt{\mathbf{C}_2(\mathbf{A})} + 1} \right)^{k+1}.^{2} \tag{6}$$

[1] $||\mathbf{x}||_{\mathbf{A}} = \sqrt{(\mathbf{x},\mathbf{x})_{\mathbf{A}}} = \sqrt{\mathbf{x}^T\mathbf{Ax}}$.

[2] The condition number $\mathbf{C}_2(\mathbf{A})$ is defined as $\mathbf{C}_2(\mathbf{A}) = \frac{\sqrt{\lambda_{max}(\mathbf{A}^T\mathbf{A})}}{\sqrt{\lambda_{min}(\mathbf{A}^T\mathbf{A})}}$. If $\mathbf{A}$ is SPD, $\mathbf{C}_2(\mathbf{A}) = \frac{\lambda_{max}(\mathbf{A})}{\lambda_{min}(\mathbf{A})}$.

Algorithm 1 Conjugate Gradient (CG) method, solving $\mathbf{Ax} = \mathbf{b}$.

```
Give an initial guess $\mathbf{x}^0$.
Compute $\mathbf{r}^0 = \mathbf{b} - \mathbf{Ax}^0$ and set $\mathbf{p}^0 = \mathbf{r}^0$.
  for $k = 0, \ldots,$ until convergence
    $\alpha^k = \frac{(\mathbf{r}^k, \mathbf{r}^k)}{(\mathbf{Ap}^k, \mathbf{p}^k)}$
    $\mathbf{x}^{k+1} = \mathbf{x}^k + \alpha^k \mathbf{p}^k$
    $\mathbf{r}^{k+1} = \mathbf{r}^k - \alpha^k \mathbf{Ap}^k$
    $\beta^k = \frac{(\mathbf{r}^{k+1}, \mathbf{r}^{k+1})}{(\mathbf{r}^k, \mathbf{r}^k)}$
    $\mathbf{p}^{k+1} = \mathbf{r}^{k+1} + \beta^k \mathbf{p}^k$
  end
```

Preconditioning

If we want to accelerate the convergence of an iterative method, we can transform the system into another one containing a better spectrum, i.e, a smaller condition number. This can be done by multiplying the original system (4) by a matrix $\mathbf{M}^{-1}$.

$$\mathbf{M}^{-1}\mathbf{Ax} = \mathbf{M}^{-1}\mathbf{b}. \tag{7}$$

The new system has the same solution but provides a substantial improvement on the spectrum. For this preconditioned system, the convergence is given by:

$$||\mathbf{x} - \mathbf{x}^{k+1}||_{\mathbf{A}} \leq 2||\mathbf{x} - \mathbf{x}^0||_{\mathbf{A}} \left(\frac{\sqrt{\mathbf{C}(\mathbf{M}^{-1}\mathbf{A})} - 1}{\sqrt{\mathbf{C}(\mathbf{M}^{-1}\mathbf{A})} + 1} \right)^{k+1}. \tag{8}$$

$\mathbf{M}$ is an *SPD* matrix chosen such that $\mathbf{C}(\mathbf{M}^{-1}\mathbf{A}) \leq \mathbf{C}(\mathbf{A})$, and $\mathbf{M}^{-1}b$ is easy to compute.

Deflation

Deflation is used to annihilate the effect of extreme eigenvalues on the convergence of an iterative method ([11]). Given an *SPD* matrix $\mathbf{A} \in \mathbb{R}^{n \times n}$, the deflation matrix $\mathbf{P}$ is defined as follows ([9]):

$$\mathbf{P} = \mathbf{I} - \mathbf{AQ}, \qquad \mathbf{P} \in \mathbb{R}^{n \times n}, \qquad \mathbf{Q} \in \mathbb{R}^{n \times n},$$

where

$$\mathbf{Q} = \mathbf{ZE}^{-1}\mathbf{Z}^T, \qquad \mathbf{Z} \in \mathbb{R}^{n \times m}, \qquad \mathbf{E} \in \mathbb{R}^{m \times m},$$

with

$$\mathbf{E} = \mathbf{Z}^T\mathbf{AZ}.$$

The matrix $\mathbf{E}$ is known as the *Galerkin* or *coarse* matrix that has to be invertible. If $\mathbf{A}$ is *SPD* and $\mathbf{Z}$ is full rank then $\mathbf{E}$ is invertible. The full rank matrix $\mathbf{Z}$ is called the $deflation - subspace$ matrix, and it's $l < n$ columns are the $deflation$ vectors or $projection$ vectors.
Some properties of the previous matrices are ([9, pag. 27]):

a) $\mathbf{P}^2 = \mathbf{P}$.

b) $\mathbf{AP}^T = \mathbf{PA}$.

c) $(\mathbf{I} - \mathbf{P}^T)\mathbf{x} = \mathbf{Qb}$.

d) $\mathbf{PAZ} = \mathbf{0}^{n \times m}$.

e) **PA** is *SPSD*[3].

We can split the vector **x** as:

$$\mathbf{x} = \mathbf{I}\mathbf{x} - \mathbf{P}^T\mathbf{x} + \mathbf{P}^T\mathbf{x} = (\mathbf{I} - \mathbf{P}^T)\mathbf{x} + \mathbf{P}^T\mathbf{x}. \tag{9}$$

Multiplying the expression above by **A**, using the properties above, we have:

$$\begin{aligned} \mathbf{A}\mathbf{x} &= \mathbf{A}(\mathbf{I} - \mathbf{P}^T)\mathbf{b} + \mathbf{A}\mathbf{P}^T\mathbf{x}, && \mathit{Property}: \\ \mathbf{A}\mathbf{x} &= \mathbf{A}\mathbf{Q}\mathbf{b} + \mathbf{A}\mathbf{P}^T\mathbf{x}, && c) \\ \mathbf{b} &= \mathbf{A}\mathbf{Q}\mathbf{b} + \mathbf{P}\mathbf{A}\mathbf{x}, && b), \end{aligned}$$

multiplying by **P** and using the properties $\mathbf{PAQ} = \mathbf{0}^{n\times n}$ and $\mathbf{P}^2 = \mathbf{P}$, properties *d*) and *e*), we have:

$$\begin{aligned} \mathbf{PAQb} + \mathbf{P}^2\mathbf{Ax} &= \mathbf{Pb}, \\ \mathbf{PAx} &= \mathbf{Pb}, \end{aligned} \tag{10}$$

where $\mathbf{PAx} = \mathbf{Pb}$ is the deflated system. Since **PA** is singular, the solution **x** can contain components of the null space of **PA**. A solution to this system, called deflated solution, is denoted by $\hat{\mathbf{x}}$. The deflated system for $\hat{\mathbf{x}}$ is:

$$\mathbf{PA}\hat{\mathbf{x}} = \mathbf{Pb}. \tag{11}$$

As mentioned above, the solution to Equation (10) can contain components of $\mathscr{N}(\mathbf{PA})$. Therefore, a solution to Equation (11), $\hat{\mathbf{x}}$ can be decomposed as:

$$\hat{\mathbf{x}} = \mathbf{x} + \mathbf{y}, \tag{12}$$

with $\mathbf{y} \in \mathscr{R}(\mathbf{Z}) \subset \mathscr{N}(\mathbf{PA})$, and **x** the solution to Equation (4).
Note: If $\mathbf{y} \in \mathscr{R}(\mathbf{Z})$, then

$$\mathbf{y} = \sum_{i=1}^{m} \alpha_i \mathbf{z}_i,$$

$$\mathbf{PA}y = \mathbf{PA}(\mathbf{z}_1\alpha_1 + \ldots + \mathbf{z}_m\alpha_m) = \mathbf{PAZ}\alpha, \tag{13}$$

from h) $\mathbf{PAZ} = \mathbf{0}^{n\times l}$, then

$$\mathbf{PAy} = \mathbf{0}. \tag{14}$$

Therefore $\mathscr{R}(\mathbf{Z}) \subset \mathscr{N}(\mathbf{PA})$.
Multiplying Equation (12) by $\mathbf{P}^T$ we obtain:

$$\mathbf{P}^T\hat{\mathbf{x}} = \mathbf{P}^T\mathbf{x} + \mathbf{P}^T\mathbf{y},$$

combining Equation (14) with f), we have:

$$\mathbf{PA}y = \mathbf{AP}^T\mathbf{y} = \mathbf{0}.$$

Therefore

$$\mathbf{P}^T\hat{\mathbf{x}} = \mathbf{P}^T\mathbf{x}. \tag{15}$$

Substitution to Equation (15) and g) in Equation (9) leads to:

$$\mathbf{x} = \mathbf{Qb} + \mathbf{P}^T\hat{\mathbf{x}}, \tag{16}$$

which gives us a relation between $\hat{\mathbf{x}}$ and **x**.

[3]Symmetric Positive Semi-Definite, $(\mathbf{Ax},\mathbf{x}) \geq 0$, for all **x**.

Deflated CG Method

To obtain the solution to the linear system (4), we solve the deflated system:

$$\mathbf{PA\hat{x}} = \mathbf{Pb}. \tag{17}$$

with the CG method, for a deflated solution $\mathbf{\hat{x}}$. Therefore, the solution $\mathbf{x}$ to the original system is obtained from (16):

$$\mathbf{x} = \mathbf{Qb} + \mathbf{P}^T\mathbf{\hat{x}}.$$

Deflated PCG Method

The deflated linear system can also be preconditioned by an *SPD* matrix $\mathbf{M}$.
The deflated preconditioned system to solve with CG is [9, pag. 30]:

$$\tilde{\mathbf{P}}\tilde{\mathbf{A}}\hat{\tilde{\mathbf{x}}} = \tilde{\mathbf{P}}\tilde{\mathbf{b}},$$

where:

$$\tilde{\mathbf{A}} = \mathbf{M}^{-\frac{1}{2}}\mathbf{A}\mathbf{M}^{-\frac{1}{2}}, \qquad \hat{\tilde{\mathbf{x}}} = \mathbf{M}^{\frac{1}{2}}\hat{\mathbf{x}}, \qquad \tilde{\mathbf{b}} = \mathbf{M}^{-\frac{1}{2}}\mathbf{b}$$

This method is called the Deflated Preconditioned Conjugate Gradient *DPCG* method, and the error is bounded by:

$$||\mathbf{x} - \mathbf{x}^{i+1}||_{\mathbf{A}} \leq 2||\mathbf{x} - \mathbf{x}^0||_{\mathbf{A}} \left(\frac{\sqrt{\mathbf{C}_{eff}(\mathbf{M}^{-1}\mathbf{PA})} - 1}{\sqrt{\mathbf{C}_{eff}(\mathbf{M}^{-1}\mathbf{PA})} + 1} \right)^{i+1},$$

were $\mathbf{C}_{eff} = \frac{\lambda_{max}(M^{-1}PA)}{\lambda_{min}(M^{-1}PA)}$ is the effective condition number and $\lambda_{min}(M^{-1}PA)$ is the smallest non-zero eigenvalue of $M^{-1}PA$.

Choices of Deflation Vectors

The deflation method is used to treat the most unfavorable eigenvalues of $\mathbf{A}$. If the matrix $\mathbf{Z}$ contains eigenvectors corresponding to the unfavorable eigenvalues, the convergence of the iterative method is achieved faster. However, to obtain and to apply the eigenvectors is costly in most of the cases. Therefore, a good choice of the matrix $\mathbf{Z}$ that does not contain the eigenvectors is essential for the acceleration of the convergence.
A good choice of the deflation vectors is usually problem-dependent. Available information on the system is, in general, used to obtain these vectors. Most of the techniques used to choose deflation vectors are based on approximating eigenvectors, recycling ([2]), subdomain deflation vectors ([12]) or multigrid and multilevel based deflation techniques ([10, 8]). A summary of these techniques is given below.

Recycling Deflation. A set of vectors previously used is reused to build the deflation-subspace matrix ([2]). The vectors could be, for example, $q-1$ solution vectors of the linear system with different right-hand sides or of different time steps. The matrix $\mathbf{Z}$ containing this solutions is:

$$\mathbf{Z} = [\mathbf{x}^{(1)}, \mathbf{x}^{(2)}, ..., \mathbf{x}^{(q-1)}].$$

Subdomain Deflation. The domain is divided into several subdomains, each corresponding to one or more deflation vectors. For each subdomain, there is a deflation vector that has ones for points in the subdomain and zeros for points outside ([12]).

Multi Grid and Multilevel Deflation. For the multigrid and multilevel methods, there are matrices called prolongation and restriction matrices that allow us to pass from one level or grid to another. These matrices are used as the deflation-subspace matrices $\mathbf{Z}$ ([10]).

Proper Orthogonal Decomposition (POD)

The Proper Orthogonal Decomposition (POD) method is a Model Order Reduction (MOR) method, where a high-order model is projected onto the space spanned by a set of orthonormal basis vectors. The high dimensional variable $\mathbf{x} \in \mathbb{R}^n$ is approximated by a linear combination of $l << n$ orthonormal basis vectors [1]:

$$\mathbf{x} \approx \sum_{i=1}^{l} z_i \phi_i, \tag{18}$$

where $\phi_i \in \mathbf{R}^n$ are the basis vectors and z_i are their corresponding coefficients. In matrix notation, equation (18) is rewritten as :

$$\mathbf{x} \approx \Phi \mathbf{z},$$

where $\Phi = [\phi_1 \ \phi_2 \ .. \ \phi_l]$, $\Phi \in \mathbf{R}^{n \times l}$ is the matrix containing the basis vectors, and $\mathbf{z} \in \mathbf{R}^l$ is the vector containing the coefficients of the basis vectors.
The basis vectors are computed from a set of 'snapshots' $\{\mathbf{x_i}\}_{i \in \mathbb{N}}$, obtained by simulation or experiments [5]. In POD, the basis vectors $\{\phi_j\}_{j=1}^{l}$, are l eigenvectors corresponding to the largest eigenvalues $\{\lambda_j\}_{j=1}^{l}$ of the data snapshot correlation matrix $\mathbf{R}$.

$$\mathbf{R} := \frac{1}{m}\mathbf{X}\mathbf{X}^T \equiv \frac{1}{m}\sum_{i=1}^{m} \mathbf{x}_i \mathbf{x}_i^T, \qquad \mathbf{X} := [\mathbf{x}_1, \mathbf{x}_2, ... \mathbf{x}_m], \tag{19}$$

where $\mathbf{X} \in \mathbf{R}^{n \times m}$ is an SPSD matrix containing the previously obtained snapshots. The l eigenvectors should contain almost all the variability of the snapshots. Usually, they are chosen as the eigenvectors of the maximal number (l) of eigenvalues satisfying [5]:

$$\frac{\sum_{j=1}^{l} \lambda_j}{\sum_{j=1}^{m} \lambda_j} \leq \alpha, \qquad 0 < \alpha \leq 1, \tag{20}$$

with α close to 1. The eigenvalues are ordered from large to small with λ_1 the largest eigenvalue of $\mathbf{R}$.

Results

Numerical experiments.

These experiments are performed in order to understand the behavior of the Deflated Conjugate Gradient method preconditioned with Incomplete Cholesky (DICCG) and to find good deflation vectors for the given problems. We propose the use of snapshots and the snapshots-based basis functions of POD as deflation vectors.
In the present section, we give a general overview of the experiments that we perform, but the specifications are presented below for each problem separately. The reference solution is obtained with a direct solution method. This solution is visually compared with the results obtained with the iterative solvers. We observed that a good choice of snapshots, and therefore of deflation vectors, depends on the boundary conditions of the problem. Hence, we study two cases with different boundary conditions. For the first set of problems, Dirichlet boundary conditions are used for an academic layered model with various contrasts in permeability between the layers. In the second set of problems, we used Neumann boundary conditions (no-flux) for the previous academic layered problem and for the SPE 10 benchmark problem. We investigate the behavior of the ICCG and DICCG methods with various contrasts between the permeability layers for both cases.
We study the influence of the size of the problem in the performance of the ICCG and DICCG methods changing the grid size of the second layer of the SPE 10 benchmark. We also investigate the performance of the above-mentioned methods with various tolerance values for the solvers. This study was performed for the second layer and for the complete SPE 10 benchmark (85 layers). We also investigate the influence of the accuracy of the snapshots in the performance of the DICCG method for the complete SPE 10 benchmark.

The model

The experiments simulate flow through porous media with a constant porosity field of 0.2. An incompressible single-phase model is studied for a fluid with the following properties:

- $\mu = 1cp$
- $\rho = 1014kg/m^3$

We model incompressible single-phase flow through porous media. The system of equations that describes this flow is given by Equation (4).

In these experiments, a Cartesian grid with different grid sizes is used. Wells or sources are added to the system. Neumann and Dirichlet boundary conditions are imposed. For some problems, a pressure drop is imposed in the y direction (Dirichlet boundary condition), and for others, the no-flux (Neumann) boundary condition is used. More specifications are presented below for each problem. The matrices corresponding to the linear systems $\mathbf{A}$ and right-hand sides $\mathbf{b}$ are obtained with MRST [6].

Snapshots

As mentioned above, for the DICCG method we need a set of deflation vectors. In a first series of experiments, the deflation vectors are solutions of the system with various well configurations and boundary conditions. These solutions, called snapshots, are obtained with ICCG, the tolerance used is given for each problem. The configuration used to obtain each snapshot depends on the problem that we are solving. For each case, the configuration of the snapshots, as well as the configuration of the system to solve, are presented.

The solver

The solution of the system is approximated with ICCG and DICCG.

For the DICCG method, we need a set of deflation vectors. For the first case (Dirichlet and Neumann boundary conditions), snapshots are used as deflation vectors. For the second case (Neumann boundary conditions only), snapshots and basis vectors of POD are used as deflation vectors. The tolerance or stopping criterium is taken as the 2-norm of the residual for the k^{th} iteration divided by the 2-norm of the right-hand side of the preconditioned system:

$$\frac{||\mathbf{M}^{-1}r^k||_2}{||\mathbf{M}^{-1}b||_2} \leq \varepsilon.$$

The stopping criterium is varied for each problem.

POD deflation vectors

The POD method requires a basis for the projection of the high-order model. This basis contains the eigenvectors corresponding to the largest eigenvalues of the data snapshot correlation matrix $\mathbf{R}$, as defined in Equation (19).

In the second set of experiments (Neumann boundary conditions only), we use snapshots and the eigenvectors corresponding to the two largest eigenvalues of the matrix $\mathbf{R}$ as deflation vectors. The $\mathbf{x}_i' s$ of the matrix $\mathbf{R}$ are the snapshots described in previous section. When we use POD deflation vectors for the DICCG method, we use the subscript $_{POD}$, i.e. the solver is DICCG$_{POD}$.

Case 1, Dirichlet and Neumann boundary conditions.
In the configuration of *Case 1*, four wells are positioned in a square at distances equal to one-third of the reservoir length and width. Two wells have a bottom hole pressure (bhp) of 5 bars, and two have a bhp of -5 bar. No-flux conditions are used at the right and left boundaries and a pressure drop in the vertical direction. The pressure at the lower boundary ($y = 1$) is 0 bars, and at the upper boundary ($y = ny$) is 3 bars. The first four snapshots ($z_1 - z_4$) are obtained setting only one well pressure different from zero, taking no-flux conditions at the right and left boundaries and homogeneous Dirichlet conditions at the other boundaries. A fifth snapshot is obtained setting all the wells pressures to zero and setting a pressure drop in the vertical direction used for the original system. A summary is presented below.

Configuration 1:

System configuration

W1 = W2 = -5 bars.

W3 = W4 = +5 bars.

Boundary conditions :

$P(y=1) = 0$ bars, $P(y=ny) = 3$ bars, $\frac{\partial P(x=1)}{\partial n} = \frac{\partial P(x=nx)}{\partial n} = 0.$

Snapshots

$\mathbf{z}_1$: W1 = -5 bars, W2 = W3 = W4 = 0,

$\mathbf{z}_2$: W2 = -5 bars, W1 = W3 = W4 = 0.

$\mathbf{z}_3$: W3 = +5 bars, W1 = W2 = W4 = 0.

$\mathbf{z}_4$: W4 = +5 bars, W1 = W2 = W3 = 0.

Boundary conditions for the first 4 snapshots:

$P(y=1) = P(y=ny) = 0$ bars, $\frac{\partial P(x=1)}{\partial n} = \frac{\partial P(x=nx)}{\partial n} = 0.$

$\mathbf{z}_5$: W1 = W2 = W3 = W4 = 0.

Boundary conditions for the 5th snapshot:

P(y=1) = 0 bars, P(y=ny) = 3 bars, $\frac{\partial P(x=1)}{\partial n} = \frac{\partial P(x=nx)}{\partial n} = 0.$

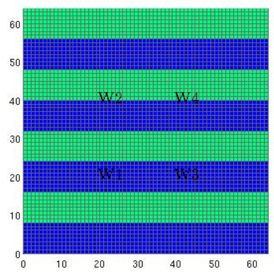

Figure 1: Heterogeneous permeability.

As mentioned above, we studied flow through a porous medium with *heterogeneous permeability* layers. A grid of $nx = ny = 64$ elements is studied. We use 8 layers of the same size, 4 layers with one value of permeability κ_1, followed by a layer with a different permeability value κ_2. The permeability of one set of layers is set to $\kappa_1 = 1mD$, the permeability of the other set κ_2 is changed. Therefore, the contrast in permeability between the layers ($\frac{\kappa_2}{\kappa_1} = \frac{\kappa_2}{1mD}$), depends on the value of κ_2.

We investigate the dependence on the contrast in permeability value between the layers for the ICCG and DICCG methods. The permeability of one set of layers is $\kappa_1 = 1mD$ in all cases, whereas the permeability of the other set of layers varies from $\kappa_2 = 10^{-1}mD$ to $\kappa_2 = 10^{-7}mD$. Figure 1 shows these layers. The tolerance is set as 10^{-11} for the snapshots as well as for the original problem.
Table 1 shows the condition number for the matrix A, the preconditioned matrix $(M^{-1}A)$ and the deflated and preconditioned matrix $(M^{-1}PA)$ for various permeability contrasts between the layers.

κ_2 (mD)	10^{-1}	10^{-3}	10^{-5}	10^{-7}
$\mathbf{C}(A)$	2.6×10^3	2.4×10^5	2.4×10^7	2.4×10^9
$\mathbf{C}(M^{-1}A)$	206.7	8.3×10^3	8.3×10^5	8.3×10^7
$\mathbf{C}_{eff}(M^{-1}PA)$	83.27	6×10^3	1×10^6	6×10^7

Table 1: Table with the condition number for the matrix obtained solving the layered problem with various permeability contrasts between the layers. Original system, preconditioned system and preconditioned and deflated system with five snapshots as deflation vectors (DICCG). Grid size of 32 x 32, $\kappa_1 = 1mD$.

Table 2 shows the number of iterations required to achieve convergence for ICCG and DICCG, for various permeability contrasts between the layers.[4]
The solution is not reached when the value of permeability is greater than $\kappa_2 = 10^{-3}$ for both methods (ICCG and DICCG). For the ICCG method the solution is completely different from the solution obtained with a direct solver, whereas for the DICCG the solution is similar, but not the same. The plot of the residual and the solution to the problem are presented in Figures 2 and 3 for a value of permeability $\kappa_2 = 10^{-3}$.
As long as the correct solution is achieved ($\kappa_2 = 10^{-1}, 10^{-3}$), we note that the number of iterations increases when the contrast between the permeability layers increases for ICCG. For DICCG, we observe that we only need one iteration despite the change in permeability contrast between the layers.

κ_2 (mD)	10^{-1}	10^{-3}	10^{-5}	10^{-7}
ICCG	75	110	22*	22*
DICCG	1	1	10	4**

Table 2: Table with the number of iterations for different contrasts in the permeability of the layers for the ICCG and DICCG methods.

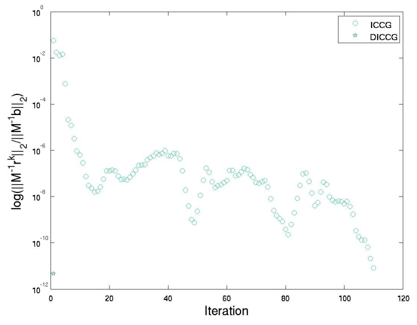

Figure 2: Convergence for the heterogeneous problem, 64 x 64 grid cells, $\kappa_2 = 10^{-3}mD$.

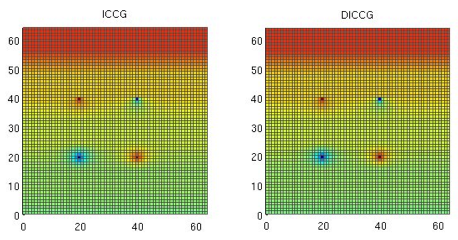

Figure 3: Solution of the heterogeneous problem, 64 x 64 grid cells, $\kappa_2 = 10^{-3}mD$.

[4]The * means that the solution is not achieved (from the plot of the solution). Meanwhile, ** means that the solution is close to the solution obtained with a direct solver.

To better understand the cases when the solution has not been achieved, we study the error of the approximations. If we want the relative error $e = \frac{||\mathbf{x}-\mathbf{x}^k||_2}{||\mathbf{x}||_2}$, with $\mathbf{x}$ the true solution and $\mathbf{x}^k$ the approximation, to be less than 10^{-7}, we need to choose a stopping criteria (tol) so that $tol = e/\mathbf{C}_2(M^{-1}A)$ for the preconditioned system, and $tol = e/\mathbf{C}_{eff}(M^{-1}PA)$ for the deflated and preconditoned system (see Apendix 1). The tolerance is presented in Table 3 for the ICCG and DICCG methods. We observe that the required tolerance (tol) when $\kappa_2 = 10^{-5}mD, 10^{-7}mD$ is smaller than our choice $(tol = 10^{-11})$. As a consequence, we cannot expect to find a correct solution for these cases.

κ_2 (mD)	10^{-1}	10^{-3}	10^{-5}	10^{-7}
$tol = \frac{e}{\mathbf{C}(M^{-1}A)}$	5×10^{-9}	1×10^{-10}	1×10^{-12}	1×10^{-14}
$tol = \frac{e}{\mathbf{C}_{eff}(M^{-1}PA)}$	1×10^{-8}	2×10^{-10}	1×10^{-12}	2×10^{-14}

Table 3: Table with the tolerance for various permeability contrasts between the layers, grid size of 32 x 32, $\kappa_1 = 1mD$.

As we see from Table 3, the tolerance required when $\kappa_2 = 10^{-5}mD$ is in the order of 10^{-12}. Therefore, if we use this tolerance we can find the solution. Tolerance for the snapshots as well as for the solver is varied. We study 3 cases, in the first case, the tolerance of the snapshots and the solvers is 10^{-12}. In the second case, the tolerance of the snapshots is reduced to 10^{-14}. Finally, in case 3 the tolerance of the solvers is reduced to 10^{-13}. Table 4 shows the number of iterations necessary to achieve convergence for ICCG and DICCG for a given tolerance (Tol solver). The solution obtained with all the methods is visually compared with the solution obtained with a direct solver.
For ICCG, the solution obtained in the first two cases is similar to the expected solution but it is not the same which indicates that a tolerance of 10^{-13} is necessary to find the solution. For DICCG, in the first case, the solution is reached after eleven iterations. If we increase the accuracy of the snapshots (Case 2) we reach the correct solution for DICCG in one iteration (the dependence on the accuracy of the snapshots for the DICCG method is studied for the SPE 10 model in the next section). If we increase the accuracy of the solvers (Case 3), the solution is also achieved, but we note that for the deflation methods the number of iterations increases.

Case	1	2	3
Tol snapshots	1×10^{-12}	1×10^{-14}	1×10^{-14}
Tol solver	1×10^{-12}	1×10^{-12}	1×10^{-13}
ICCG	55^{**}	55^{**}	94
DICCG	11	1	2

Table 4: Number of iterations for ICCG, DICCG for a layered problem, $\kappa_1 = 1mD$, $\kappa_2 = 10^{-5}mD$, grid size of 64x 64.

Case 2, Neumann boundary conditions only.
In this case, four wells are positioned in the corners and have a bhp of -1 bar. One well is positioned in the center of the domain and has a bhp of +4 bars (see Figure 4). We set Neumann boundary conditions in all boundaries. The snapshots ($z_1 - z_4$) are obtained giving a value of zero to one well and non zero values to the other wells. A summary of the configurations is presented below.

Configuration 2:

System configuration

W1 = W2 = W3 = W4 = -1 bar.

W5 = +4 bars.

Boundary conditions :

$$\frac{\partial P(y=1)}{\partial n} = \frac{\partial P(y=ny)}{\partial n} = \frac{\partial P(x=1)}{\partial n} = \frac{\partial P(x=nx)}{\partial n} = 0.$$

Snapshots

$\mathbf{z}_1$: W1 = 0 bars, W2 = W3 = W4 = -1 bars, W5 = +3 bars.

$\mathbf{z}_2$: W2 = 0 bars, W1 = W3 = W4 = -1 bars, W5 = +3 bars.

$\mathbf{z}_3$: W3 = 0 bars, W1 = W2 = W4 = -1 bars, W5 = +3 bars.

$\mathbf{z}_4$: W4 = 0 bars, W1 = W2 = W3 = -1 bars, W5 = +3 bars.

Boundary conditions

$$\frac{\partial P(y=1)}{\partial n} = \frac{\partial P(y=ny)}{\partial n} = \frac{\partial P(x=1)}{\partial n} = \frac{\partial P(x=nx)}{\partial n} = 0.$$

Heterogeneous permeability layers
As in the previous case, single-phase flow through a porous medium with heterogeneous permeability layers is studied. A grid of $nx = ny = 64$ elements is investigated. The deflation vectors used in this case are the 4 snapshots ($\mathbf{z}_1$-$\mathbf{z}_4$) and two basis vectors obtained for the POD method.
The snapshots and the solutions are obtained with a tolerance of 10^{-11}.

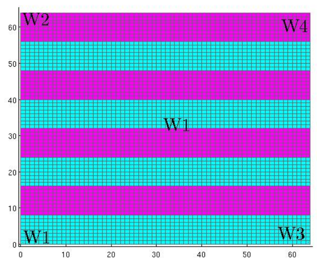

Figure 4: Heterogeneous permeability.

Table 5 shows the number of iterations required to achieve convergence for ICCG, DICCG with four snapshots as deflation vectors and DICCG$_{POD}$ with 2 POD basis vectors as deflation vectors. The plot of the residual and the solution of the problem are presented in Figure 5 and 6 for the ICCG and DICCG methods.
As in Case 1, we note that the solution is not achieved when the permeability coefficient κ_2 is smaller

than 10^{-3} for all the solvers. We can also observe that the performance of DICCG and DICCG$_{POD}$ is similar. Therefore, in the analysis of the results, we will refer only to DICCG for both solvers. Studying solely the correct solutions for ICCG, the number of iterations increases as the contrast in the permeability increases. For the DICCG method, convergence is reached within one iteration.

κ_2	10^{-1}	10^{-3}	10^{-5}	10^{-7}
ICCG	90	131	65*	64*
DICCG	1	1	1*	1*
DICCG$_{POD}$	1	1	1*	1*

Table 5: Table with the number of iterations for different contrast in the permeability of the layers for the ICCG, DICCG and DICCG$_{POD}$ methods, tolerance of solvers and snapshots 10^{-11}.

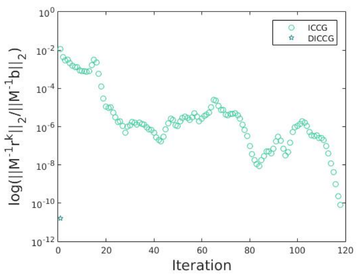

Figure 5: Convergence for the heterogeneous problem, 64 x 64 grid cells, $\kappa_2 = 10^{-3}$.

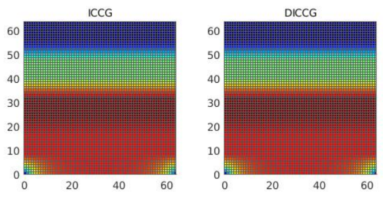

Figure 6: Solution of the heterogeneous problem, 64 x 64 grid cells, $\kappa_2 = 10^{-3}$.

To better understand the utility of POD we present an example with a larger number of snapshots, and we use the POD basis vectors to reduce this number. We solve the heterogeneous layered case with layers of permeability $\kappa_1 = 1mD$ and $\kappa_2 = (10^{-1}, 10^{-3})$ mD. In this case, we use 15 snapshots that are not linearly independent. These snapshots are the following:

Snapshots

$\mathbf{z}_1$: W1 = W2 = W3 = W4 = -1 bars, W5 = +4 bars.

$\mathbf{z}_2$: W1 = 0 bars, W2 = W3 = W4 = -1 bars, W5 = +3 bars.

$\mathbf{z}_3$: W2 = 0 bars, W1 = W3 = W4 = -1 bars, W5 = +3 bars.

$\mathbf{z}_4$: W3 = 0 bars, W1 = W2 = W4 = -1 bars, W5 = +3 bars.

$\mathbf{z}_5$: W4 = 0 bars, W1 = W2 = W3 = -1 bars, W5 = +3 bars.

$\mathbf{z}_6$: W1 = W2 = 0 bars,W3 = W4 = -1 bars, W5 = +2 bars.

$\mathbf{z}_7$: W2 = W3 = 0 bars, W1 = W4 = -1 bars, W5 = +2 bars.

$\mathbf{z}_8$: W3 = W4 = 0 bars, W1 = W2 = -1 bars, W5 = +2 bars.

$\mathbf{z}_9$: W1 = W3 = 0 bars, W2 = W4 = -1 bars, W5 = +2 bars.

$\mathbf{z}_{10}$: W2 = W4 = 0 bars, W1 = W3 = -1 bars, W5 = +2 bars.

$\mathbf{z}_{11}$: W1 = W4 = 0 bars, W2 = W3 = -1 bars, W5 = +2 bars.

$\mathbf{z}_{12}$: W1 = -1 bars, W2 = W3 = W4 = 0 bars, W5 = +1 bars.

$\mathbf{z}_{13}$: W2 = -1 bars, W1 = W3 = W4 = 0 bars, W5 = +1 bars.

$\mathbf{z}_{14}$: W3 = -1 bars, W1 = W3 = W4 = 0 bars, W5 = +1 bars.

$\mathbf{z}_{15}$: W4 = -1 bars, W1 = W2 = W3 = 0 bars, W5 = +1 bars.

Boundary conditions

$$\frac{\partial P(y=1)}{\partial n} = \frac{\partial P(y=ny)}{\partial n} = \frac{\partial P(x=1)}{\partial n} = \frac{\partial P(x=nx)}{\partial n} = 0.$$

With these snapshots, we compute the data snapshot correlation matrix $\mathbf{R} = \mathbf{X}\mathbf{X}^T$, where the rows of $\mathbf{X}$ are the snapshots presented above. We compute the eigenvalues of the correlation matrix, they are presented in Figure 7. We observe that the first four eigenvalues are close to 10^8 orders of magnitude larger than the rest of the eigenvalues. Our deflation vectors are the eigenvectors corresponding to these four eigenvalues. The number of iterations necessary to achieve convergence is presented in Table 6

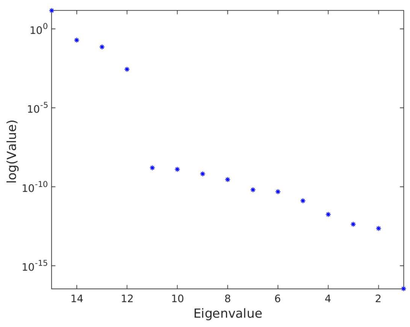

Figure 7: Eigenvalues of the snapshot correlation matrix $\mathbf{R} = \mathbf{X}\mathbf{X}^T$, 15 snapshots used.

for the ICCG and the deflated method. For the deflated method, 15 snapshots were used as deflation vectors DICCG$_{15}$, and the eigenvectors corresponding to the 4 largest eigenvalues of the matrix $\mathbf{R}$ (see Figure 7). We observe that for the deflated method, when we use the 15 snapshots, the correct solution is not achieved after 500 iterations, the maximum number of iterations allowed for this problem. For this problem we have a linearly dependent set of snapshots, causing that the Galerkin matrix ($\mathbf{E} = \mathbf{Z}^T\mathbf{A}\mathbf{Z}$) is close to singular such that it cannot be accurately inverted, a requirement for a good performance of the deflation method. As a result, the deflation method does not work properly. However, when we use 4 of the basis vectors of POD, we achieve the solution within one iteration. In this example, we reduce the number of snapshots from 15 to 4 using the basis vectors of POD, selecting in this way the dominant features of the system.

κ_2	10^{-1}	10^{-3}
ICCG	90	131
DICCG$_{15}$	500*	500*
DICCG$_{POD}$	1	1

Table 6: Table with the number of iterations for different contrast in the permeability of the layers for the ICCG, DICCG$_{15}$ and DICCG$_{POD}$ methods, tolerance of solvers and snapshots 10^{-11}.

SPE 10 model (1 layer)

This model has large variations in the permeability coefficients. It contains 60 x 220 x 85 cells, in this section only one layer (2nd) is used (60 x 220 x 1 cells). This model has 5 sources or wells, four producers in the corners (negative) and one injector in the center (positive).

The snapshots are obtained solving the system with different well configurations (*Configuration 2*). Four snapshots are used as deflation vectors. As before, we simulate single-phase incompressible flow. The dependence of the DICCG method on the accuracy of the snapshots is investigated. Snapshots are obtained with different accuracy, the values of tolerance used are 10^{-1}, 10^{-3}, 10^{-5}, and 10^{-7}. The original system is solved with an accuracy of 10^{-7}. In the first experiment with the deflation method, the four snapshots are used as deflation vectors (DICCG). In the second, 2 vectors of the POD basis are used as deflation vectors (DICCG$_{POD}$).

Different grid sizes are studied: 16 x 56, 30 x 110, 46 x 166 and 60 x 220.

Permeability is upscaled averaging the permeability in each grid using the harmonic-arithmetic average algorithm from MRST. The permeability of the coarser grid (16 x 56 cells) is shown in Figure 8. The permeability contrast for the diverse grid size problems is shown in Table 7. From this table, we observe that the contrast in the permeability for different grid sizes varies slightly, but that the order of magnitude remains the same for all the cases.

The condition number for the coarse grid problem (16 x 56) is studied in Table 8 for the original system, the preconditioned system and the deflated and preconditioned system with four snapshots as deflation vectors. In this table we observe an important reduction in the condition number for the preconditioned the system and a further reduction when the system is deflated.

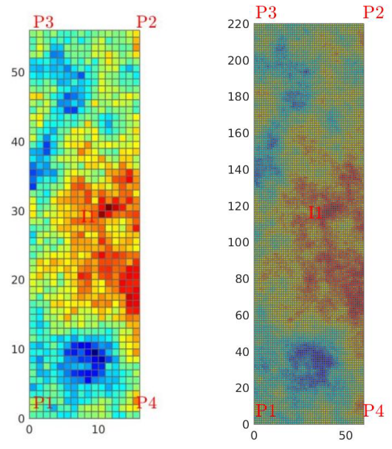

(a) 16 x 56 grid cells (b) 60 x 220 grid cells

Figure 8: Permeability field, 16 x 56 and 60 x 220 grid cells.

Grid size	16 x 56	30 x 110	46 x 166	60 x 220
Contrast ($\times 10^7$)	1.04	2.52	2.6	2.8

Table 7: Table with the contrast of permeabilities for different grid sizes.

The number of iterations required to achieve convergence with the ICCG, DICCG and DICCG$_{POD}$ methods for various grid sizes and various accuracy values of the snapshots is presented in Table 9.

As in the previous experiment, the number of iterations is similar for the DICCG and DICCG$_{POD}$ methods, therefore we will analyze only the solutions obtained with DICCG, as the same analysis holds for DICCG$_{POD}$.

The convergence and the solution to the ICCG and DICCG methods with a tolerance of the snapshots of 10^{-7} are presented in Figure 9 and Figure 10. For ICCG, the required iterations to reach convergence increases as the size of the grid increases. We note that the accuracy of the snapshots is important for the

Condition number	Value
$\mathbf{C}(A)$	2.2×10^6
$\mathbf{C}(M^{-1}A)$	377
$\mathbf{C}_{eff}(M^{-1}PA)$	82.7

Table 8: Table with the condition number of the matrix obtained for the SPE 10 model. Original system, preconditioned system and preconditioned and deflated system with four snapshots as deflation vectors (DICCG). Grid size of 16 x 56.

DICCG method. When the accuracy is low, the DICCG method behaves almost as the ICCG method, as the accuracy increases, the number of iterations diminishes. We observe that, if we use the same accuracy for the snapshots and the solver, 10^{-7}, the solution is reached within one iteration.

Tol	Method	16 x 56	30 x 110	46 x 166	60 x 220
	ICCG	34	73	126	159
10^{-1}	DICCG	33	72	125	158
	DICCG$_{POD}$	33	72	125	158
10^{-3}	DICCG	18	38	123	151
	DICCG$_{POD}$	21	40	123	153
10^{-5}	DICCG	11	21	27	55
	DICCG$_{POD}$	11	21	27	48
10^{-7}	DICCG	1	1	1	1
	DICCG$_{POD}$	1	1	1	1

Table 9: Table with the number of iterations for ICCG, DICCG and DICCG$_{POD}$, various tolerance for the snapshots, various grid sizes.

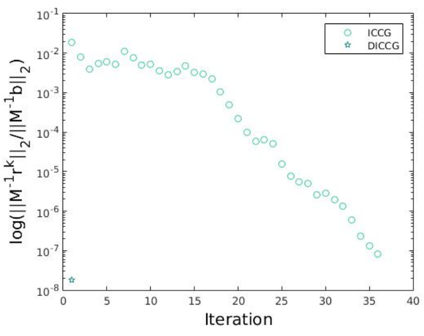

Figure 9: Convergence for the SPE 10 problem, 16 x 56 grid cells, accuracy of the snapshots 10^{-7}.

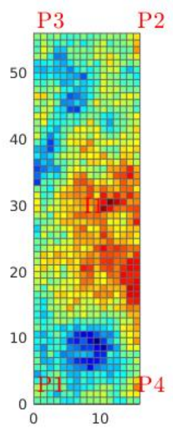

Figure 10: Solution of the SPE 10 benchmark, 16 x 56 grid cells, 2nd layer, accuracy of the snapshots 10^{-7}.

SPE 10 complete
We approximate the solution for the complete SPE 10 benchmark (60 x 220 x 65) with the ICCG and DICCG methods (see Figure 11). The contrast in permeability between the layers for this problem is 3×10^{-7}. We use four deflation vectors, $z_1 - z_4$ ($Configuration$ 2). The accuracy of the snapshots is varied from 10^{-2} to 10^{-11} in steps of 10^{-3}. For the solution, accuracy is varied from 10^{-5} to 10^{-11} in steps of 10^{-3}. Results are presented in Table 10. The convergence plot is presented in Figure 12 and the solution in Figure 13 for an accuracy of the snapshots and solvers of 10^{-11}.
We observe from Table 10, that the number of iterations necessary to achieve convergence is the same for ICCG and DICCG if the accuracy of the snapshots is low (tol 10^{-2}). When the accuracy improves, the number of iterations is reduced for DICCG. Convergence is achieved within one iteration for DICCG when the accuracy of the snapshots is 10^{-11}. This is a significant improvement with respect to ICCG which needs 1029 iterations to achieve the solution.
We also observe that, if the accuracy of the solver is not good enough, the correct solution is not reached. This should be linked to the condition number of the matrix of the problem, and the required accuracy for the solvers. As the problem is very large in this case, an analysis of the condition number is not possible. However, we know that the contrast between the permeability layers is of the order of 10^{-7}, and from the heterogeneous problem we can see that in this case, it is possible that the reduction of the condition number is not large enough, and therefore, the required accuracy is not reached.

Tol. sol	10^{-5}	10^{-8}	10^{-11}
Tolerance of snapshots 10^{-2}			
ICCG	165*	610*	1029
DICCG	163*	604*	1029
DICCG$_{POD}$	164*	551*	1029
Tolerance of snapshots 10^{-5}			
ICCG	165*	610*	1029
DICCG	1*	467**	878
DICCG$_{POD}$	8*	465*	872
Tolerance of snapshots 10^{-8}			
ICCG	165*	550*	1030
DICCG	1*	1*	564
DICCG$_{POD}$	1*	1*	475
Tolerance of snapshots 10^{-11}			
ICCG	165*	572*	1029
DICCG	1	1	1
DICCG$_{POD}$	1	1	1

Table 10: Table with the number of iterations for different accuracy in the snapshots and the solution obtained with the ICCG, DICCG and DICCG$_{POD}$ methods.

For this problem, we also study the behaviour of the DICCG method with 15 linearly dependent snapshots. The snapshots used are the same as the snapshots used for the heterogeneous permeability case (with 15 snapshots). The accuracy for the snapshots and the solvers is 10^{-11}.
The eigenvalues of the data snapshot correlation matrix $\mathbf{R} = \mathbf{X}\mathbf{X}^T$ are presented in Figure 14. The number of iterations necessary to achieve the desired tolerance for the ICCG and DICCG methods is

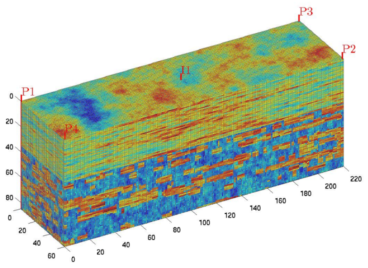

Figure 11: SPE 10 benchmark, permeability field.

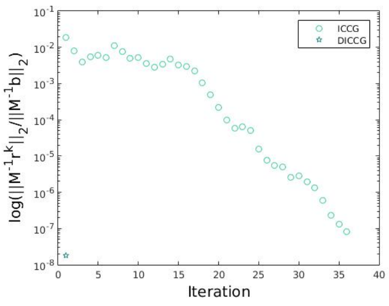

Figure 12: Convergence for ICCG and DICCG, SPE 10 model, 85 layers, accuracy of the snapshots 10^{-11}.

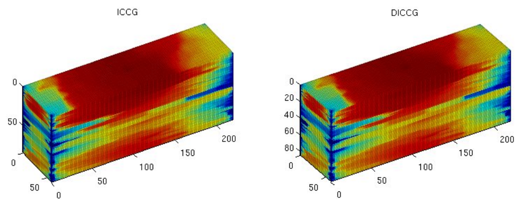

Figure 13: Solution to the SPE 10 model (85 layers) with ICCG and DICCG, tolerance of the snapshots and solvers 10^{-11}.

ICCG	1011
DICCG$_{15}$	2000
DICCG$_{POD}$	2

Table 11: Table with the number of iterations for different contrast in the permeability of the layers for the ICCG, DICCG$_{15}$ and DICCG$_{POD}$ methods, tolerance of solvers and snapshots 10^{-11}.

presented in Table 11. For the deflated method we use 15 snapshots as deflation vectors (DICCG$_{15}$), and the eigenvectors corresponding to the four largest eigenvalues (1-4) of the matrix $\mathbf{R}$.

We observe in Table 11 that for the deflated method, when we use the 15 snapshots, the correct solution

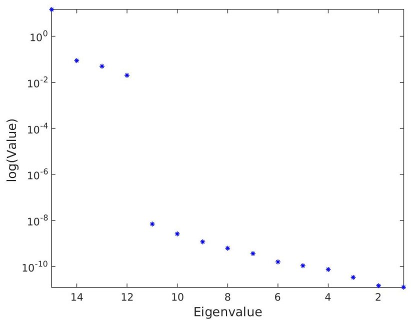

Figure 14: Eigenvalues of the snapshot correlation matrix $\mathbf{R} = \mathbf{X}\mathbf{X}^T$, 15 snapshots used.

is not reached after 2000 iterations, the maximum number of iterations allowed for this problem. As mentioned for the layered problem with Neumann boundary conditions, this behaviour is caused by the dependence of the snapshots. If we use 4 of the basis vectors of POD, we reach the solution within two iterations. As in the heterogeneous permeability problem, we reduce the number of snapshots from 15 to 4 using the basis vectors of POD and we reach the solution after a small number of iterations.

Conclusions

Single-phase flow of an incompressible fluid through porous media with high-contrast in the permeability field is studied. We study an academic layered problem and the SPE 10 benchmark. For the solution of these problems, we propose a selection of physics-based deflation vectors to be used with the Deflated Conjugated Gradient preconditioned with Incomplete Cholesky (DICCG) method.
Results show that the choice of deflation vectors is important for a good performance of the method and that the correct choice depends on the boundary conditions. The proposed deflation vectors are based on snapshots, solutions of the system with some variations on the right-hand side.
Snapshots are selected taking into account the sources, wells in this case, and the boundary conditions. When Dirichlet boundary conditions are used, vectors related to the wells and a vector related to the boundary conditions should be used. In the case of Neumann boundary conditions, only snapshots related to the wells are used. Snapshots are used as deflation vectors in the case of Dirichlet and Neumann boundary conditions.
For the case with Neumann boundary conditions only, snapshots and basis vectors of POD are used as deflation vectors. For the first set of experiments with the layered and SPE 10 problems, the number of snapshots depends on the number of wells, in these examples four snapshots are used. Results show that the performance of the DICCG method is similar when we use four snapshots or two basis vectors of POD as deflation vectors in all the studied examples of Neumann boundary conditions only. Although the number of snapshots is not large, in problems that require a larger number of snapshots to capture the dynamics of the system, POD vectors could be useful to reduce this number. As an example, we solve the heterogeneous layered problem and the complete SPE 10 problem with a larger number of snapshots. We reduce the original set of 15 snapshots to 4 basis vectors of POD.
Results also show that the accuracy of the snapshots used as deflation vectors is essential for the correct performance of the DICCG method. For an academic layered problem, we note that the contrast between the layers modifies the condition number and demands a higher accuracy for the solvers.
We also observe that if the accuracy of the snapshots is not ’good’ enough, the solution of the original system with the deflated method is reached, but the number of iterations is large, in some cases is the same as for the ICCG method. As the accuracy of the snapshots is improved, the number of iterations is reduced for the deflated method. For the cases when the correct accuracy is used for the snapshots, the DICCG method reaches the solution within one iteration.
Results also show that the performance of the solver DICCG does not depend on the grid size (SPE 10 example with one layer) or on the contrast between permeability layers (academic layered problem), when a correct accuracy for the snapshots and the solver is used.

Appendix 1. Stopping criteria

When we use an iterative method, we always want that our approximation is close enough to the exact solution. In other words, we require that the error [7, pag. 42]:

$$||\mathbf{e}^k||_2 = ||\mathbf{x} - \mathbf{x}^k||_2,$$

or the relative error:

$$\frac{||\mathbf{x} - \mathbf{x}^k||_2}{||\mathbf{x}||_2},$$

is small.
When we want to chose a stopping criteria, we could think that the relative error is a good candidate, but is has the disadvantage that we need to know the exact solution to compute it. What we have instead is the residual

$$\mathbf{r}^k = \mathbf{b} - \mathbf{A}\mathbf{x}^k,$$

that is actually computed in each iteration of the CG method. There is a relationship between the error and the residual that can help us with the choice of the stopping criteria.

$$\frac{||\mathbf{x} - \mathbf{x}^k||_2}{||\mathbf{x}||_2} \leq \mathbf{C}_2(A)\frac{||\mathbf{r}^k||_2}{||\mathbf{b}||_2}.$$

With this relationship in mind, we can choose the stopping criteria as an ε for which

$$\frac{||\mathbf{r}^k||_2}{||\mathbf{b}||_2} \leq \varepsilon.$$

But we should keep to have in mind the condition number of the matrix $\mathbf{A}$, because the relative error will be bounded by:

$$\frac{||\mathbf{x} - \mathbf{x}^k||_2}{||\mathbf{x}||_2} \leq \mathbf{C}_2(A)\varepsilon.$$

Acknowledgements (Optional)

We want to thank the Mexican Insitute of Petroleum (IMP) that through the program: ’Programa de Captación de Talento, Reclutamiento, Evaluación y Selección de Recursos Humanos (PCTRES)’ has sponsored this work.

References

[1] P. Astrid, G. Papaioannou, J. C. Vink and J.D. Jansen. [2011] *Pressure Preconditioning Using Proper Orthogonal Decomposition*. Paper SPE 141922 presented at the SPE Reservoir Simulation Symposium, The Woodlands, USA, 21-23 February.

[2] M. Clemens, M. Wilke, R. Schuhmann and T. Weiland. [2004] *Subspace projection extrapolation scheme for transient field simulations*. IEEE Transactions on Magnetics. **40**(2), 934-937.

[3] M.A. Christie, and M.J. Blunt. [2001] Tenth SPE Comparative Solution Project: a Comparison of Upscaling Techniques. SPE Reservoir Engineering and Evaluation **4** (4): 308-317.

[4] J. D. Jansen. [2013] *A systems description of flow through porous media.* New York: Springer.

[5] R. Markovinović and J. D. Jansen. [2006] *Accelerating iterative solution methods using reduced-order models as solution predictors*. International journal for numerical methods in engineering. **68**(5), 525-541.

[6] K. A. Lie. [2013] *An Introduction to Reservoir Simulation Using MATLAB: User guide for the Matlab Reservoir Simulation Toolbox (MRST)*. SINTEF ICT.

[7] Y. Saad. [2003] *Iterative Methods for Sparse Linear Systems*. Society for Industrial and Applied Mathematics Philadelphia.

[8] B. Smith, P. Bjorstad, W. Gropp. [1996] *Domain decomposition: parallel multilevel methods for elliptic partial differential equations*. Cambridge University Press New York.

[9] J.M. Tang. [2008] *Two-Level Preconditioned Conjugate Gradient Methods with Applications to Bubbly Flow Problems*. PhD Thesis, Delft University of Technology.

[10] J.M. Tang, R. Nabben, C. Vuik and Y. Erlangga. [2009] *Comparison of two-level preconditioners derived from deflation, domain decomposition and multigrid methods*. Journal of scientific computing. **39**(3), 340-370.

[11] C. Vuik, A. Segal and J. A. Meijerink. [1999] *An Efficient Preconditioned CG Method for the Solution of a Class of Layered Problems with Extreme Contrasts in the Coefficients*. Journal of Computational Physics. **152**, 385-403.

[12] C. Vuik, A. Segal, L. Yaakoubi and E. Dufour. [2002] *A comparison of various deflation vectors applied to elliptic problems with discontinuous coefficients*. Applied Numerical Mathematics. **41**(1), 219.